The Sherwood number of a bubble rising in oil

F.Peters[1]*, M.Nüllig[1]

[1]Ruhr Universität Bochum, Fluid Mechanics, 44801 Bochum, Germany

*franz.peters@rub.de

Abstract

Oil holds remarkable amounts of gas which may be exchanged with bubbles. We investigate the rate at which bubbles dissolve in stagnant oil when rising at their natural velocity. Our experimental method is the rotary chamber. It allows levitation and observation of the rising bubble. Bubble sizes from 1 to 8mm are covered. The saturation rate of the oil ranges from zero to fully saturated. Results are produced in terms of the Sherwood number vs. Archimedes number. Most notable is the detection of a transformation of the interface with a considerable impact on the Sherwood number.

1 Introduction

Bubbles in water have been of predominant interest over decades, see Clift et al.(1978), because they are ubiquitous and readily made. Also the bubble-water interface is special due to the high surface tension and the high attraction to surfactants. However, there are other important systems and applications. In process engineering and lubrication technology bubbles play an important role because oil interchanges a lot of gas with bubbles carried along. Real vapor cavitation is a different process, yet it may interact with gas bubbles. To a large extent mass transfer at gas bubbles is controlled by diffusion. This has been widely overlooked mainly because diffusion is labelled too slow to play a role in cavitation. Peters and Honza (2014) as well as Groß and Pelz (2017) have conducted seminal experiments to rethink the problem.

The present work deals with a reduced, elementary experiment on bubbles in oil. We study at what rate single bubbles of different gases (mainly argon, oxygen or nitrogen) dissolve into oil when they rise at their natural velocity. Besides the rate we determine the velocity itself, the bubble deformation and the state of the interface, whether it moves with the flow (mobile) or remains stagnant (immobile). The mass transfer results appear in dimensionless form based on the scaling parameters Sherwood number and Archimedes number. A clear view is obtained on the relation between bubble properties and mass transfer. All this is made possible by the rotary chamber technique which has been employed successfully in our group by Nüllig and Peters(2013, 2014). The key advantage of the chamber is that a bubble can be observed over its life time in a levitated position.

All experiments were carried out in mineral white oil taken from one batch (Meguin PP20 DAB10). Not available physical properties were measured.

2 Experimental

We have been working with rotary chambers for various goals among them the bubble diffusion rate in water, e.g Nüllig and Peters (2016). Presently a follow-up version like in Fig.1 was employed. Two round plates made from acrylic glass are kept at a distance of 76 mm by a PVC-ring. This way we get a drum like chamber including a volume of 6.3 liter. The stability of the drum and the parallelism of the plates is achieved by an outer frame held together by an array of bolts. Filling and draining of the chamber takes place via a single port through the PVC-ring (not shown) which is closed by a small plug. The chamber is supported by two rubber coated rollers which are driven by a frequency controlled motor. Rotational chamber speeds were 1.83 rad/s for nitrogen and 1.90 rad/s for the other gases.

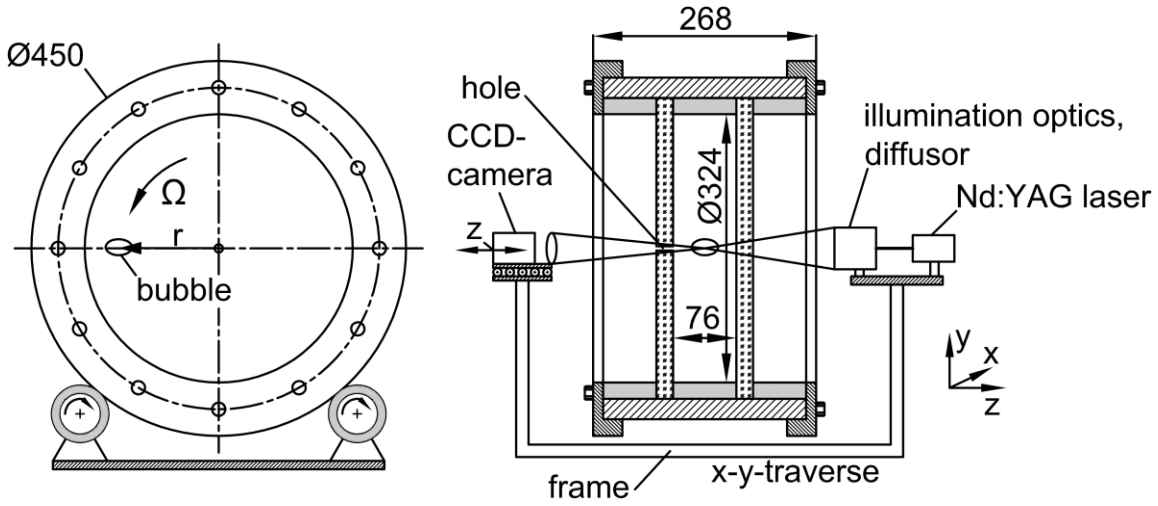

Fig. 1 Rotary chamber in side view (left) and cross view (dimensions in mm).

Bubbles are introduced into the rotating chamber through a small center hole in one of the side plates. A special syringe operating with capillaries allows the predetermination of the bubble volume V and an injection like bubble release. For more details on chamber operation, bubble generation, bubble release and capillary size see Nüllig and Peters (2013, 2014, 2016). The hole remains exposed to atmospheric pressure at all times except for filling. It is small enough for a stable meniscus and big enough to neglect the capillary pressure. After injection the bubble performs a few loops before it levitates at some radial position close to the horizontal line. In this position forces in radial and tangential direction are equilibrated as shown by Nüllig and Peters (2018).

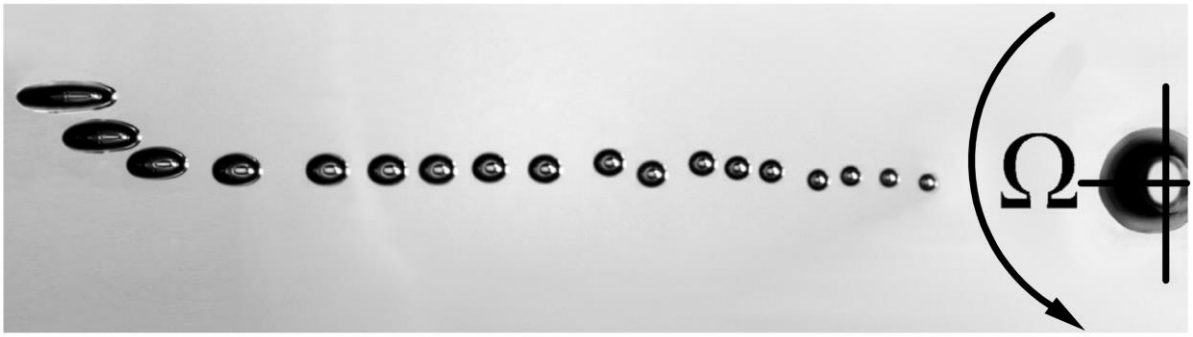

Fig. 2 Sequence of images as the bubble proceeds in undersaturated oil from left to right towards the center of rotation.

Fig. 2 presents a sequence of bubble images vs. time. The chamber rotates counter-clockwise about the crossing point. The process of diffusion starts at the left edge with a large, deformed bubble of known initial volume. On its way to the center it loses volume and approaches a spherical shape. Bubble position and shape are observed by a CCD-camera (*LaVision Imager pro X 4M*) with high resolution (2048 x 2048 pixel). Illumination is provided by a diffuse light plate pulsed by a Nd:YAG laser (*Solo III, New Wave*). The arrangement of light source and camera is shown in Fig. 1. Light source and camera are fixed with respect to each other. They can be moved on an x-y-traverse to trace the bubble position with respect to the center of rotation. The images are stored in an IMX-format and evaluated using MATLAB tools.

The evaluation of the mass transfer is based on the precise determination of the bubble volume as it shrinks with time, see Nüllig and Peters (2014). The initial volume comes along with the syringe injection.

3 Results

Fig. 3 shows an example of recorded $d_e(t)$ traces for argon. χ is the saturation ratio. The bubbles were launched somewhat above 8 mm such that recording could begin at 8 mm. All traces show a similar behavior. A constant initial slope bends over to a smaller slope which is also constant.

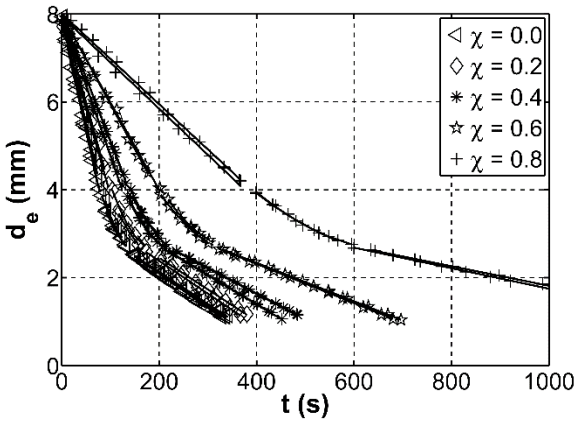

Fig. 3. Recorded d_e (from the equivalent spherical volume) for argon at different saturation ratios χ (χ=0 is totally degassed.)

The Sherwood Sh number takes the form

$$Sh = \frac{\rho_{in}}{(\rho_\infty - \rho_s)D} d_e \frac{dR}{dt}$$

which is normally plotted against the Reynolds number. With respect to buoyancy we prefer the Archimedes number as discussed by Peters and Gärtner (2011) which reads

$$Ar = \frac{g\, d_e^3}{\nu_{ex}^2}$$

With the Ostwald coefficient L one gets $Sh = C\, Ar^{1/3}$ where dR/dt remains constant. C is

$$C = \left(\frac{\nu_{ex}^2}{g}\right)^{1/3} \cdot \frac{dR/dt}{L\,(\chi - 1)\,D}$$

		argon	oxygen	nitrogen
bubble size	χ	C	C	C
	(-)	(-)	(-)	(-)
8 (7.4) to 4 mm	0.0	32.382	57.653	25.612
	0.2	32.490	58.021	26.043
	0.4	32.266	58.077	25.785
	0.6	31.838	59.117	26.066
	0.8	32.708	56.162	26.732
2.7 to 1 mm	0.0	4.735	9.909	6.068
	0.2	6.034	11.989	5.987
	0.4	6.612	12.403	6.328
	0.6	6.969	13.492	5.936
	0.8	7.160	13.066	5.930

Tab. 1 Calculated values for C. Note that C>0 because dR/dt and (χ-1) are negative.

Fig.4 displays the results as Sh(Ar) in a log-log plot. The five χ-traces for each gas appear now collectively bundled over an order of magnitude of the higher Archimedes numbers. For the smaller Archimedes numbers the five curves appear somewhat spread within the dark bars (nitrogen and argon

share the black bar). In both ranges the proportionality $Sh \propto Ar^{1/3}$ is observed as indicated by the inserted line. In total the Sherwood number extends over 2 orders of magnitude when going from large to small bubbles. Therefore, the relative mass transfer at a big bubble is a hundred times more effective than the one at a small bubble. Note that oxygen features by far the greatest Sherwood number followed by argon and nitrogen.

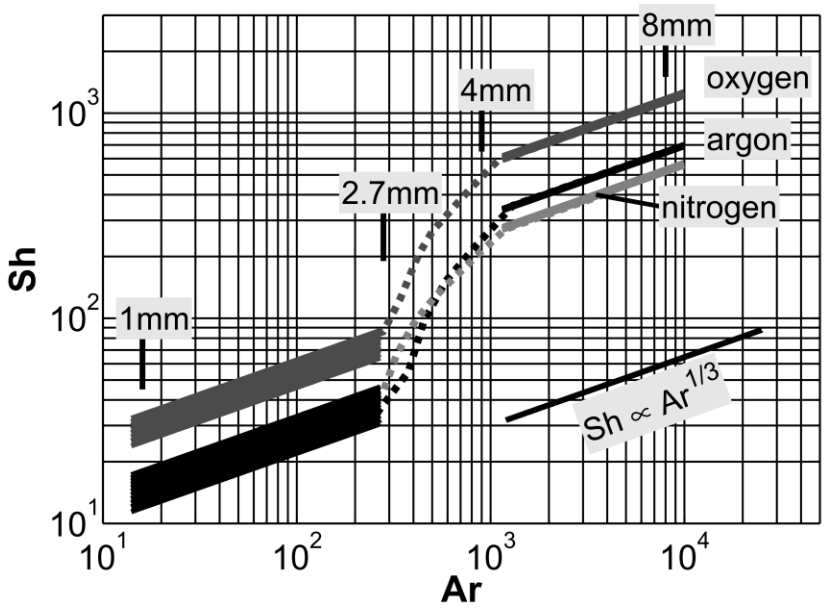

Fig. 8. Sh vs. Ar for oxygen, argon and nitrogen bubbles dissolving in white oil.

The substantial transition of Sh between 2.7 mm to 4 mm is unusual and not straightforward. In the progress of the experiments we convinced ourselves that the transition is unambiguously related to the state of the boundary condition at the bubble surface. It means that a mobile surface at a large bubble gradually stiffens in the transition zone (decreasing bubble volume) to become an immobile surface. Although the principal existence of a transition has been proved for water by Nüllig and Peters (2018) we find no immediate indication in this experiment. The line of argument to follow is to consider the bubble rise velocity and corresponding drag coefficients. This has been shown by Nüllig and Peters (2018).

The relatively wide transition zone means that the immobilization from large to small bubbles takes place gradually. The spread of the data within the bars suggests that the process is not perfectly reproducible. All this agrees with the cap formation concept suggested by Levich (1962). Obviously, we are not in the position to identify a mechanism which creates the cap. Using clean oil there is no clue on impurities and after all a self-structuring of the oil molecules can hardly be ruled out.

4 Conclusion

Gas bubbles rising in white oil were investigated with respect to mass transfer rates by a rotary chamber technique. The main free variables concerned the kind of gas and the pre-saturation of the oil (five pre-saturations). Bubble sizes were limited to 0.3 mm (equivalent diameter) at the lower end due to experimental conditions and 8 mm at the upper end set by a natural instability of the bubbles.

Mass transfer rates were deduced from size vs time. Already there two rate levels were observed bridged by a transition. The corresponding presentation in the Sherwood-Archimedes diagram shows a striking result. Large bubbles above the transition zone feature high Sherwood numbers proportional to $Ar^{1/3}$. This dependency holds also for small bubbles below the transition. Yet the level of the Sherwood number appears significantly lower than predicted by an extension of the upper curve. The explanation of this behavior was found to be the change of the bubble interface. The large bubbles start with a mobile

interface which changes to immobile within the transition zone. Most likely this is caused by impurities which form a cap and gradually change the boundary conditions for flow and mass transfer. Therefore, from the perspective of the immobile interface the mobile interface enhances the normalized mass transfer substantially.

Acknowledgements

This project was supported by the Mercator Research Center Ruhr (MERCUR) which is gratefully acknowledged.

References

Clift R, Grace J R, Weber M E (1978) Bubbles, drops, and particles. Academic Press, New York

Peters F and Honza R. (2014) A benchmark experiment on gas cavitation. Experiments in Fluids 55: 1786

Groß, T. F.; Pelz P. F. (2017) Diffusion-driven nucleation from surface nuclei in hydrodynamic cavitation. J. Fluid Mech. 830: 138-164

Nüllig M and Peters F (2013) Diffusion of small gas bubbles into liquid studied by the rotary chamber technique. Chemie Ingenieur Technik 85, No. 7: 1074–1079

Nüllig M and Peters F (2014) Zur Ermittlung von Blasenvolumina. Chemie Ingenieur Technik 86, No. 11: 1981–1985

Nüllig M and Peters F (2016) Diffusion of large nitrogen bubbles into tap water studied by the rotary chamber technique. Chemie Ingenieur Technik 88, No. 8: 1151–1156

Nüllig M and Peters F (2018) Experiments on the mass transfer of gas bubbles in mineral oil. Colloids and Surfaces A 540: 81-89

Peters F and Gaertner B. (2011) Scaling parameters of bubbles and drops; interpretation and case study with air in silicon oil. Acta Mechanica 219:189–202

Nüllig M and Peters F (2018) Experiments on the transition of fast to slow bubbles in water. Chemical Engineering Science 175: 91-97

Levich V.G. (1962) Physicochemical hydrodynamics. Prentice Hall